

DTI studies in patients with Alzheimer's disease, mild cognitive impairment, or normal cognition with evaluation of the intrinsic background gradients

Geon-Ho Jahng · Songfan Xu · Micheal W. Weiner ·
Dieter J. Meyerhoff · Seungjoon Park · Norbert Schuff

Received: 25 September 2010 / Accepted: 1 February 2011 / Published online: 22 February 2011
© The Author(s) 2011. This article is published with open access at Springerlink.com

Abstract

Introduction The objective of the study was to explore the impact of the background gradients on diffusion tensor (DT) magnetic resonance imaging (DT-MRI) in patients with Alzheimer's disease (AD), mild cognitive impairment (MCI), or cognitively normal (CN) aging.

Methods Two DT-MRI sets with positive and negative polarities of the diffusion-sensitizing gradients were obtained in 15 AD patients, 18 MCI patients, and 16 CN control subjects. The maps of mean diffusivity (MD) and fractional anisotropy (FA) were computed separately for

positive (p: pMD and pFA) and negative (n: nMD and nFA) polarities, and we computed the geometric mean (gm) of the DT-MRI to obtain the gmFA and gmMD with reducing the background gradient effects. Regional variations were assessed across the groups using one-way analysis of variance.

Results Increased regional gmMD values in the AD subjects, as compared to the regional gmMD values in the MCI and CN subjects, were found primarily in the frontal, limbic, and temporal lobe regions. We also found increased nMD and pMD values in the AD subjects compared to those values in the MCI and CN subjects, including in the temporal lobe and the left limbic parahippocampal gyrus white matter. Results of comparisons among the three methods showed that the left limbic parahippocampal gyrus and right temporal gyrus were the increased MD in the AD patients for all three methods.

Conclusion Background gradients affect the DT-MRI measurements in AD patients. Geometric average diffusion measures can be useful to minimize the intrinsic local magnetic susceptibility variations in brain tissue.

Keywords Diffusion tensor imaging · Background gradients · Alzheimer's disease · Mild cognitive impairment · Geometric mean analysis

G.-H. Jahng (✉)

Department of Radiology,
Kyung Hee University Hospital-Gangdong,
School of Medicine, Kyung Hee University,
149 Sangil-dong, Gangdong-gu,
Seoul 134-727, South Korea
e-mail: ghjahng@gmail.com

S. Xu · S. Park

Department of Biomedical Science,
Graduate School of Kyung Hee University,
1 Hoegi-dong, Dongdaemun-gu,
Seoul 130-701, South Korea

M. W. Weiner · D. J. Meyerhoff · N. Schuff

Center for Imaging of Neurodegenerative Diseases,
VA Medical Center and the Department of Radiology,
University of California-San Francisco,
4150 Clement Street, 114M,
San Francisco, CA 94121, USA

S. Park

Department of Pharmacology and the Medical Research Center
for Bioreaction to ROS and the Biomedical Science Institute,
School of Medicine, Kyung Hee University,
1 Hoegi-dong, Dongdaemun-gu,
Seoul 130-701, South Korea

Introduction

Diffusion tensor (DT) magnetic resonance imaging (DT-MRI) is sensitive to the directionality of the random motion of water in tissue, and it involves the application of external diffusion-sensitizing magnetic field gradients along different orientations to quantify the properties of diffusion.

Numerous DT-MRI studies of neurodegenerative diseases have reported abnormal diffusion values in the brain, including Alzheimer's disease (AD), which is a devastating condition that leads to progressive memory loss and rapid cognitive decline. Although AD is generally considered to affect primarily the gray matter, several studies have found changes of the isotropic and anisotropic diffusion in white matter associated with AD progression by using DT-MRI [1–6]. The diffusion abnormalities in AD were predominantly found in the posterior regions of the brain such as the hippocampal gyrus, the temporal white matter, the splenium of the corpus callosum, and the posterior cingulum. In patients with mild cognitive impairment (MCI), which is considered to represent a transitional stage between normal aging and AD, the changes seem to parallel those in AD with similar posterior regions showing abnormalities. In contrast to AD and MCI, the diffusion abnormalities in subjects with age-associated changes (cognitively normal, CN) occur in the frontal regions, and specifically in the frontal white matter, the anterior cingulum, and the genu of the corpus callosum [7].

Although the marked differences seen on DT-MRI between AD or MCI and normal aging have been considered as potential imaging markers [8–10], the underlying mechanism of the DT-MRI changes remains largely unexplained. In particular, the local variations in cell density, oligodendrocytes, myelination, and also amyloid plaques, which are a hallmark of AD [11–13], can be the source of local magnetic susceptibility variations, which in turn can alter water diffusion. Furthermore, it has been shown in rat brain [14] that brain iron, which occurs in high concentrations in oligodendrocytes and plaques [15–17], can modulate the diffusion measurements. These finding suggests that local magnetic susceptibility variations in brain tissue may contribute to the DT-MRI abnormalities seen in AD and MCI in the form of intrinsic susceptibility-dependent background gradients that add to the external diffusion weighting gradients. The previous DT-MRI studies did not take into account the local variations in brain.

All investigators may be interested in knowing where in the brain and for which patients these different diffusion effects are with and without considering the background gradients. So, the overall goal of this study was to investigate whether intrinsic background gradients contribute to the pattern of regional diffusion abnormalities in patients with AD, MCI, and CN, and this potentially reflects the underlying pathological processes associated with brain iron. Specifically, we hypothesized that AD patients show a systematic pattern of higher regional background gradients compared to the MCI and CN subjects.

Materials and methods

Theoretical background

Neeman et al. [18] reported the use of diffusion-encoding schemes that were made up of couples of gradients with positive and negative polarities in order to minimize a cross-term effect in the case of static field inhomogeneities. To minimize the scalar effects of the unknown cross-term effect of the background and the diffusion-encoding gradients, the geometric mean (gm) operation was used for both the positive and negative polarities of the diffusion-encoding gradients by applying the following equations [18, 19]:

$$S_{gm} = \sqrt{S_p \cdot S_n} = S_0 \text{Exp}(-b_{gm} \cdot ADC) \quad (1)$$

$$b_{gm} = \frac{b_p + b_n}{2} = -\gamma^2 \delta^2 (aG_d^2 + bG_b^2 + cG_{img}^2 + fG_b \cdot G_{img}) \quad (2)$$

$$b_{gm} \cong -\gamma^2 \delta^2 (aG_d^2 + cG_{img}^2) \quad (3)$$

where the geometric mean operation is defined as $\sqrt{S_p \cdot S_n}$ where S_p and S_n are the signals acquired with positive (p) and negative (n) gradients polarities, S_0 is the signal acquired without a diffusion gradient, the b value = 0 s/mm², b_p is the b value with using positive diffusion gradients, b_n is the b value with using negative diffusion gradients, b_{gm} is the b value calculated by b_p and b_n , γ is the gyromagnetic ratio, δ is the duration of the externally applied diffusion gradient, G_d is the amplitude of the known diffusion-encoding gradients, G_b is an amplitude of the unknown background gradients, G_{img} is the amplitude of the known imaging gradients, and a , b , c , and f are coefficients. Please note that with this calculation, the cross terms, both $G_b \cdot G_d$ and $G_{img} \cdot G_d$, disappeared. The background gradients G_b^2 and the cross term, $G_b \cdot G_{img}$, in Eq. 2 can be ignored because those values are much smaller than G_d^2 . Therefore, the b_{gm} value can finally be considered as Eq. 3.

Subjects

Table 1 lists the demographic data of the subjects, including gender, age, and the Mini-Mental State Examination Score (MMSE), which is a general measure of cognitive performance. Fifteen patients diagnosed with AD (mean age 75 years, standard deviation (SD) 9.2, age range 61–86 years, 9 males and 6 females, MMSE range 7–28, mean MMSE 21.9) based on the National Institute of Neurolog-

Table 1 Demographic data and the neuropsychologic test results

	AD	MCI	CN
Subjects	15	18	16
Age ^a (years)	76.6 (9.1)	72.6 (8.5)	73.1 (9.5)
Gender			
Male	9	7	9
Female	6	11	7
MMSE	21.9 (5.5) ^b	28.5 (1.8)	29.3 (0.8)

AD Alzheimer's disease, MCI mild cognitive impairment, CN cognitively normal, MMSE Mini-Mental State Examination Score

The data are presented as the mean (standard deviation)

^a There are no statistically significant differences between the groups ($p > 0.05$)

^b There are statistically significant differences between the AD group and the other groups ($p < 0.0005$), but not between the MCI and CN groups ($p > 0.215$)

ical and Communicative Disorders and Stroke-Alzheimer's Disease and Related Disorder's Association (NINCDS-ADRDA) criteria were studied using a 1.5T clinical MRI system. In addition, 18 patients diagnosed with MCI (mean age 72 years, SD 8.5, age range 56–96 years, 7 males and 11 females, MMSE range 23–30, mean MMSE 28.5) and 16 CN control subjects (mean age 73 years, SD 9.5, age range 62–85 years, 9 males and 7 females, MMSE range 28–30, mean MMSE 29.3) were recruited as well. The diagnosis of MCI followed Petersen's criteria [20]. Prior to the onset of this study, informed consent was obtained from all subjects, and the protocol was approved by the local institutional review board in the USA. All experiments on human subjects were conducted in accordance with the Declaration of Helsinki.

MRI acquisition

The DT-MRI measurements were performed using a single-shot echo-planar imaging (EPI) sequence with inversion-prepared magnetization to suppress the cerebrospinal fluid (CSF) [21]. CSF suppression was used to reduce errors in the diffusion measurements from the partial volume effects in the voxels that represent CSF. A double refocusing spin-echo acquisition with bipolar external diffusion gradients [22] was employed to minimize the artifacts due to eddy currents. Six diffusion encoding directions [23] and five diffusion sensitivities (b values 0, 160, 360, 640, and 1,000 s/mm²) were acquired to determine the apparent diffusion coefficients and the diffusion tensor for each voxel. Furthermore, two DT-MRI datasets were acquired with alternating polarities of the external diffusion-sensitizing gradients (positive $+G_d$ and negative $-G_d$) to investigate the effects of background gradients on the DT-

MRI measures of the patients with AD. The other imaging parameters were as follows: repetition time (TR)/echo time (TE)/inversion time (TI)=5,000/100/3,000 ms with 2.4×2.4 mm² in-plane resolution and 19 slices of 5-mm slice thickness without a gap, which covered approximately 80% of the brain.

In addition to the DT-MRI scan, the sagittal structural volumetric T₁-weighted (T1W) images were acquired as follows: TR/TE/TI=10/4/300 ms, flip angle=15° and spatial resolution = $1 \times 1 \times 1.5$ mm resolution. The intermediate (or proton density)-weighted (PD) and T₂-weighted (T2W) axial images were also acquired using a multislice double spin-echo (DSE) sequence. The imaging parameters for DSE were as follows: TR/TE₁=5,000/20/80 ms with 1.25×1 mm in-plane resolution and a 3-mm thickness, and contiguous slices covering the entire brain. The structural images allowed registration between the structural data and the DT-MRI data and spatial normalization of the DT-MRI indices into a reference space (*vide infra*). In addition, a T₂-weighted spin-echo EPI image (referred to below as a reference EPI image) was acquired at the same resolution and orientation as the diffusion scans, but with whole brain coverage and without inversion preparation to improve registering the DT-MRI data to the structural images. Acquisition of the reference EPI was necessary because the DT-MRI slices did not cover the whole brain and the EPI data without diffusion gradients (EPI at $b=0$ s/mm²) had limited structural information because of the inversion pulse.

DT-MRI preprocessing

In order to map the diffusion indices of the mean diffusivity (MD) and the fractional anisotropy (FA) from the DT-MRI data obtained from the positive ($+G_d$) and negative ($-G_d$) diffusion-encoding gradients, we developed in house software with interactive data language (IDL; Research Systems, Inc., Boulder, CO). The MD and FA maps (pMD and pFA) were calculated by using only the positive polarity of the diffusion-encoding gradients, and these maps (nMD and nFA) were also calculated by using only the negative polarity of the diffusion-encoding gradients separately without taking into account a background gradient effect. In addition, the maps of the geometric means of MD and FA (gmMD and gmFA) were calculated to minimize the unknown cross-term effects of the background and the diffusion-encoding gradients. The geometric means of FA and MD were calculated by taking the inner product of the diffusion-encoding gradients with positive and negative polarities according to $\sqrt{S_p * S_n}$, where S_p and S_n are the diffusion-weighted signals acquired with the positive (p) and negative (n) gradient polarities, respectively [18, 19]. The calculations of the geometric

mean used the same b values as the ones used for the DT-MRI with the positive and negative diffusion-encoding gradients. A more detailed description of the geometrical mean computation can be found in the “[Theoretical background](#)” section. All the maps were calculated before performing imaging coregistration.

Postprocessing and statistical analyses

Image coregistration

The raw DT-MRI and DT_b0 EPI were assumed to be intrinsically aligned. This assumption is reasonable because first, both datasets are subjected to similar geometrical distortions; second, additional distortions due to the eddy currents induced by the diffusion-encoding gradients are minimal since we used a double refocusing sequence; and third, the datasets were acquired in an interleaved fashion to reduce movement effects between the frames. The DT_b0 EPI data (TE=100 ms and inversion-prepared and 19 slices) were coregistered to the reference EPI data (TE=100 ms without inversion, but with whole brain coverage) using an affine transformation available with Statistical Parameter Mapping software (SPM2, Wellcome Department of Cognitive Neurology, England, UK). The reference EPI data were then further coregistered to the T2W images, which were in turn coregistered to the PD images (acquired together with the T2W using double spin-echo acquisition). Finally, the PD images, and thus the DT_b0 EPI data and the maps of the DT-MRI data were coregistered to the 3D T1W images. These steps allowed a reliable coregistration between the MD and FA maps and the anatomical 3D T1W images.

Spatial normalization

A study-specific template was created by transforming the 3D T1W images from all the subjects in this study into a T1W SPM2 template space using affine transformations and by averaging all the transferred 3D T1W images provided from the SPM2 website. We created this template since our study population had brain disease and the study population was considerably older than the populations used in the standard templates, such as the Montréal Neurological Institute (MNI) template. After creating the study specific template, all the 3D T1W images from the individual subjects were again spatially normalized to this study specific template using a 12-parameter nonlinear transformation [24, 25]. The same transformation parameters were then applied to normalize all the MD and FA maps, which were also interpolated to the 2 mm×2 mm×2 mm voxel size of the brain template. The maps from the positive and negative external diffusion-sensitizing gradients (p/nFA

and p/nMD) and the corresponding maps of the geometric means (gmFA and gmMD) were then smoothed using an 8×8×12 mm Gaussian kernel.

Statistical analyses

In order to investigate the differences in diffusion abnormalities across the groups, voxel-wise one-way analysis of variance (ANOVA) tests were performed on the gmMD and gmFA maps within the framework of SPM2. These analyses were repeated for the pMD and pFA maps as well as for the nMD and nFA maps. In this analysis, we want to know where in the brain and for which patients were the gmMDs different from either the nMD or pMD. To account for multiple comparisons in the voxel-by-voxel tests, the concept of a false discovery rate (FDR) [26] was used, and a threshold for the significance of FDR $p=0.01$ was applied. Based on the results of the tests, we obtained common areas of the three MDs that were nMD, pMD, and gmMD to evaluate the advantages of the geometrical mean operation.

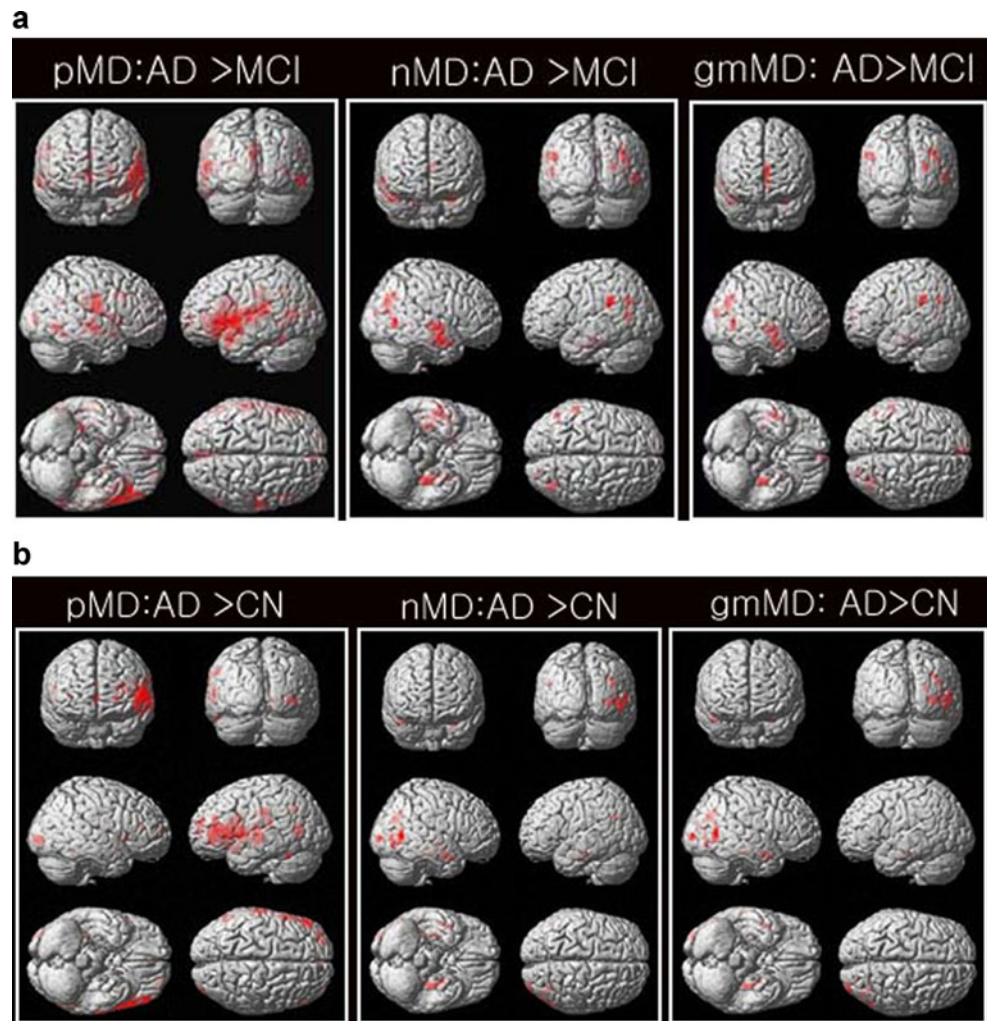
In addition to the voxel-based analyses, we also analyzed the data with defining a region-of-interest (ROI). The ROIs were defined according to the results of voxel-based analyses. For the MD, the ROIs were the right and left superior temporal gyrus (ROI1), the right and left limbic parahippocampal gyrus (ROI2), and the right and left middle temporal gyrus (ROI3) and the right and left occipital cuneus (ROI4) and the right left limbic uncus (ROI5). For the FA, the ROIs were the right and left superior temporal gyrus (ROI 6, 7, and 8) and the right and left superior frontal gyrus (ROI 9, 10). The significant level was used with $p=0.016$ ($p=0.05/3$ times repeated) because we repeated the same tasks three times among the three groups.

Results

The demographic characteristics of the subjects are summarized in Table 1. There were no significant differences in age and gender across the groups. As expected, the MMSE scores were significantly lower for the AD patients as compared to those of the other groups ($p<0.05$), but the MMSE scores did not significantly differ between the MCI and CN subjects ($p>0.05$).

Figure 1 shows the results of the voxel-wise comparisons of the pMD, nMD, and gmMD maps between the AD and MCI groups (Fig. 1a) and between the AD and CN groups (Fig. 1b) based on one-way ANOVA tests. Compared to the MCI patients, the AD patients had increased pMD values mainly in the temporal and frontal lobes. The AD patients also had increased nMD values (AD > MCI)

Fig. 1 Results of the voxel-wise comparisons of mean diffusivity (MD; *gmMD*, *nMD*, *pMD*) between the Alzheimer's disease (AD) and mild cognitive impairment (MCI) groups (a) and between the AD and cognitive normal (CN) groups (b) using one-way ANOVA tests. There were no decreased MD values for all three maps of *gmMD*, *pMD*, and *nMD* in the patients with AD as compared with that of the MCI or CN patients. There were no significant differences between the MCI and CN patients



mainly in the temporal lobe. Moreover, we found that the AD patients had increased *gmMD* values (AD > MCI) predominantly in the right superior temporal gyrus, the left limbic parahippocampal gyrus white matter, and the left superior and medial frontal gyrus. There were no significantly decreased MD values in the *gmMD*, *pMD*, and *nMD* maps from the patients with AD as compared with that of the MCI subjects. The detailed results are summarized in Table 2.

Compared to the CN subjects, the AD patients had increased *pMD* values mainly in the temporal gyrus. The AD patients also had increased *nMD* values (AD > CN) mainly in the temporal gyrus. Moreover, we found that the AD patients had increased *gmMD* values (AD > CN, Fig. 1b) predominantly in the left limbic parahippocampal gyrus, the left limbic uncus, the left and right temporal subgyrus, and the right middle temporal gyrus. These detailed results are summarized in Table 3.

Figure 2 shows the differences in the *pFA* maps between the MCI or CN and AD subjects. Compared to the MCI

patients, the AD patients had increased *pFA* values (AD > MCI) mainly in the temporal and frontal gyrus and the posterior cingulate. The detailed results are also summarized in Table 4. Compared to the CN subjects, the AD patients also had increased *pFA* values (AD > CN) mainly in the left inferior and superior frontal gyrus. We did not find any significant differences in the *pFA* between the MCI and CN subjects. Similarly, we did not find any significant differences in the *gmFA* or *nFA* across the three groups. The results of the *FA* are summarized in Table 5.

The significant regions that overlap in all three DT-MRI sets (positive gradients, negative gradients, and geometric mean) as well as those regions that differ are listed in Table 6 for the MD (*pMD*, *nMD*, and *gmMD*) and in Table 7 for the *FA* measures. The overlapping regions of increased MD in the AD patients relative to the MCI subjects (AD > MCI) included the right superior temporal gyrus and left limbic parahippocampal gyrus. In contrast, the nonoverlapping regions of increased MD in the AD patients relative to the MCI patients (AD > MCI) included:

Table 2 The significantly different regions when comparing between the AD and MCI groups (AD > MCI) using the MD with (gmMD) and without (nMD and pMD) minimizing the effects of the background gradients (corrected FDR ($p < 0.01$) as the cluster level; one-way ANOVA tests)

	Talairach coordinate			Cluster	T	Z	Region	BA ROI#
	X	Y	Z					
gm	50	-4	-22	602	5.56	5.27	R. temporal subgyrus, WM	
	50	-18	-4	602	4.83	4.64	R. superior temporal gyrus, GM	22
	58	-6	-4	602	4.8	4.61	R. superior temporal gyrus, WM	ROI1
	-32	-24	-22	264	5.32	5.07	L. limbic parahippocampal gyrus, WM	ROI2
	38	-72	32	323	4.94	4.73	R. occipital subgyrus, WM	
	-4	62	14	303	4.81	4.62	L. superior frontal gyrus, GM	9
	-4	50	20	303	4.65	4.47	L. medial frontal gyrus, WM	
	-6	62	-4	303	4.41	4.26	L. medial frontal gyrus, WM	
Neg	50	-6	-20	1,041	5.78	5.46	R. temporal subgyrus, WM	
	50	-18	-4	1,041	5.02	4.8	R. superior temporal gyrus, GM	22
	58	-6	-4	1,041	5.03	4.81	R. superior temporal gyrus, WM	ROI1
	-30	-22	-22	546	5.73	5.41	L. limbic parahippocampal gyrus, WM	
	38	-72	30	432	5.18	4.95	R. temporal subgyrus, WM	
	36	-72	6	432	3.94	3.83	R. middle occipital gyrus, WM	
	-26	-6	-32	546	4.35	4.21	L. limbic parahippocampal gyrus, WM	
	-32	2	-22	546	4.49	4.33	L. limbic parahippocampal gyrus, WM	
Pos	40	-74	30	1,759	4.82	4.63	R. middle temporal gyrus, WM	ROI3
	-4	62	10	1,024	5.38	5.11	L. medial frontal gyrus, GM	
	-4	50	20	1,024	5.44	5.17	L. medial frontal gyrus, WM	10
	-6	62	-4	1,024	5.23	4.98	L. medial frontal gyrus, WM	
	24	-86	16	1,759	5.74	5.42	R. occipital ceneus, WM	ROI4
	54	-64	6	1,759	5	4.78	R. middle temporal gyrus, WM	
	-56	-44	32	523	5.22	4.98	L. parietal supramarginal gyrus, WM	
	-50	-38	30	523	4.41	4.26	L. interior parietal lobule, WM	
	-58	-34	18	523	4.4	4.25	L. superior temporal gyrus, WM	
	-30	2	-22	732	4.49	4.33	L. limbic parahippocampal gyrus, GM	34
	-24	-4	-32	732	3.65	3.56	L. limbic uncus, WM	ROI5
	50	-4	-22	779	5.34	5.09	R. temporal subgyrus, WM	
	-32	-26	-22	732	5.01	4.79	L. limbic parahippocampal gyrus, WM	ROI2
	40	40	26	408	4.71	4.52	R. middle frontal gyrus, GM	9
	50	-6	-4	779	4.6	4.43	R. sublobar insula	
	48	30	28	408	4.52	4.36	R. middle frontal gyrus, GM	9
50	-18	-4	779	4.66	4.49	R. superior temporal gyrus, GM	22	
46	46	8	408	4.03	3.91	R. middle frontal gyrus, WM		

gm geometric mean, Neg negative, Pos positive, BA Brodmann area, R. right, L. left, WM white matter, GM gray matter

the right occipital subgyrus and the left medial and superior frontal gyrus for the gmMD; the right middle occipital gyrus for the nMD; the right middle temporal gyrus, the left medial frontal gyrus, the right occipital cuneus, the left parietal supramarginal gyrus, the left limbic parahippocampal gyrus, the left limbic uncus, the right insula, and the right middle frontal gyrus for the pMD.

Similarly, the overlapping regions of increased MD in the AD patients relative to that of the control subjects

(AD > CN) included the left limbic parahippocampal gyrus and right middle temporal gyrus. In contrast, the nonoverlapping regions of increased MD in the AD patients relative to that of the control subjects included: the left limbic uncus and the left and right temporal subgyrus for the gmMD; the left and right temporal subgyrus and the right sublobar insula for the nMD; the right temporal subgyrus, the right occipital subgyrus, the right occipital cuneus and the right inferior occipital

Table 3 The significantly different regions when comparing between the AD and CN groups (AD > CN) using the MD with (gmMD) and without (nMD and pMD) minimizing the effects of the background gradients (corrected FDR ($p < 0.01$) as the cluster level; one-way ANOVA tests)

	Talairach coordinate			Cluster	T	Z	Region	BA ROI#	
	X	Y	Z						
gm	-32	-24	-22	289	5.18	4.94	L. limbic parahippocampal gyrus, WM	ROI2	
	-26	-8	-28	289	4.32	4.18	L. limbic uncus, GM, amygdala		
	-30	0	-20	289	4.29	4.15	L. temporal subgyrus, WM		
	50	-2	-22	157	4.99	4.78	R. temporal subgyrus, WM		
	40	-74	28	530	4.9	4.7	R. middle temporal gyrus, WM		ROI3
	56	-64	8	530	4.69	4.51	R. middle temporal gyrus, WM		
	32	-66	34	530	4.59	4.42	R. temporal subgyrus, WM		
Neg	-32	-24	-22	415	5.47	5.19	L. limbic parahippocampal gyrus, WM	ROI2	
	-26	-8	-30	415	4.9	4.69	L. limbic parahippocampal gyrus, WM		
	-30	0	-20	415	4.22	4.09	L. temporal subgyrus, WM		
	50	-2	-22	294	5.09	4.86	R. temporal subgyrus, WM		
	40	-74	28	622	4.85	4.65	R. middle temporal gyrus, WM		ROI3
	34	-66	34	622	4.7	4.52	R. temporal subgyrus, WM		
	48	-18	-4	294	4.4	4.24	R. sublobar insula, GM		13
Pos	46	-60	2	622	4.47	4.31	R. temporal subgyrus, WM	ROI2	
	-32	-26	-22	409	4.87	4.67	L. limbic parahippocampal gyrus, WM		
	-28	-2	-20	409	4.45	4.29	L. limbic parahippocampal gyrus, WM		
	42	-74	28	1,010	5.22	4.95	R. middle temporal gyrus, WM		ROI3
	54	-64	8	1,010	5.28	5.03	R. middle temporal gyrus, WM		
	30	-66	34	1,010	4.81	4.62	R. occipital subgyrus, WM		ROI4
	26	-84	16	485	5.12	4.89	R. occipital cuneus, WM		
30	-94	4	485	4.73	4.55	R. occipital subgyrus, WM	ROI4		
38	-94	-2	485	4.39	4.24	R. inferior occipital gyrus, WM			

R. right, L. left

gyrus for the pMD. Because the gmFA and nFA differences between the AD patients and the other two groups of subjects were not significant, there were no overlapping regions for the FA measures.

Tables 8 and 9 list the results of ROI analyses for the MD and the FA, respectively. As we can see in the tables, MD values were significantly different between AD and MCI or between AD and CN. There was no significant difference between MCI and CN. Those results were the same as those from VBM analyses.

Discussion

A new finding of this study is that in AD patients, the background gradients have a significantly greater effect on the MD than that in the MCI or CN subjects. This finding is consistent with our hypothesis that the elevated iron-rich processes in AD patients, such as the accumulation of amyloid plaques, induce local variations in magnetic

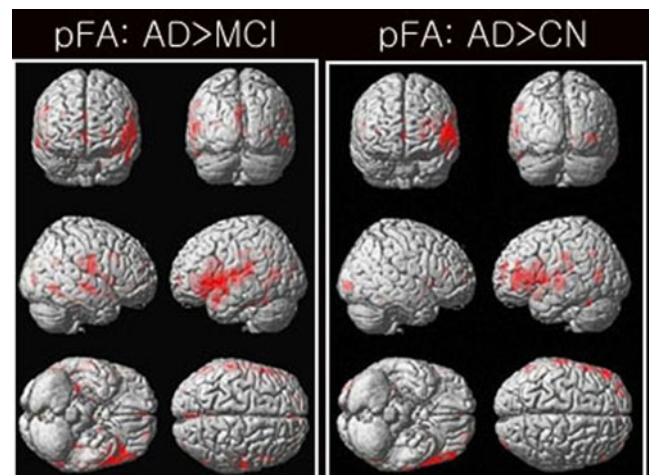


Fig. 2 Results of the voxel-wise comparisons of fractional anisotropy (FA; gmFA, nFA, pFA) among the three AD, MCI, and CN groups using one-way ANOVA tests. The pFA maps were not significantly different between the MCI and CN groups. The gmFA and nFA maps were not significantly different among the three AD, MCI, and CN groups at all

Table 4 The significantly different regions when comparing between the AD and MCI groups (AD > MCI) using the FA maps with (gmFA) and without (nFA and pFA) minimizing the effects of the background gradients (corrected FDR ($p < 0.01$) as a cluster level; one-way ANOVA tests)

	Talairach coordinate			Cluster	T	Z	Region	BA ROI#
	X	Y	Z					
gm	No significant difference							
Neg	No significant difference							
Pos	-58	-32	14	4,975	5.95	5.6	L. superior temporal gyrus, WM	ROI6
	-54	24	8	4,975	5.89	5.56	L. inferior frontal gyrus, GM	45
	52	-12	22	1,550	5.75	5.43	R. sublobar extranuclear, WM	
	50	2	10	1,550	5.46	5.18	R. sublobar insula, WM	
	38	-24	18	1,550	5.91	4.71	R. sublobar insula, GM	
	34	-30	-16	383	5.51	5.23	R. limbic parahippocampal gyrus, WM	
	50	-40	-22	383	3.9	3.79	R. temporal fusiform gyrus, GM	13
	64	-16	-6	459	4.91	4.71	R. superior temporal gyrus, WM	ROI7
	58	-26	-4	459	5.26	4.12	R. superior temporal gyrus, WM	37 ROI8
	-2	-74	26	761	4.83	4.63	L. occipital cuneus, GM	18
	-2	-60	30	761	4.65	4.47	L. limbic posterior cingulate	
	-2	-88	18	761	4.47	4.31	L. occipital cuneus, GM	18
	-56	-66	10	404	4.72	4.53	L. middle temporal gyrus, WM	
	-60	-58	2	404	4.24	4.1	L. middle temporal gyrus, WM	

R. right, L. left

susceptibility, and these are detectable as regional changes in the background gradients. This finding suggests that the contributions to the background gradients are heterogeneous. Finally, our results from the regular DT-MRI maps using diffusion-sensitizing gradients with positive polarity alone are consistent with the results of the previous DT-MRI studies on AD, MCI, and CN subjects.

AD was associated with a systematic pattern of diffusion alternations in the MD maps relative to MCI and CN even when the geometrical mean values of diffusivity (gmMD) were computed, which should in principle lead to diminished effects of the background gradients. The increased gmMD values in the AD subjects were found in the region of the right superior temporal gyrus. A previous DT-MRI study that used single polarity diffusion-encoding gradients

reported elevated MD values in the AD subjects relative to that in the MCI subjects in the same region [5]. In addition, we also found increased gmMD values in the AD subjects in the left superior frontal gyrus gray matter and left medial frontal gyrus white matter. Furthermore, compared to the CN subjects, we found increased gmMD values in the AD subjects in the limbic parahippocampal and right middle temporal gyrus, and the left and right temporal white matter. Those areas were also consistent with those of the previous single polarity DT-MRI studies in AD patients [1, 3, 4, 27]. Furthermore, we found increased gmMD values in the AD subjects involving the left limbic uncus gray matter, and this region has not been reported before in DT-MRI studies. The findings are consistent with our results of comparing the MD maps derived from

Table 5 The significantly different regions when comparing between the AD and CN groups (AD > CN) using the FA maps with (gmFA) and without (nFA and pFA) minimizing the effects of the background gradients (corrected FDR ($p < 0.01$) as a cluster level; one-way ANOVA tests)

	Talairach coordinate			Cluster	T	Z	Region	BA ROI#
	X	Y	Z					
gm	No significant difference							
Neg	No significant difference							
Pos	-48	42	-4	2,986	6.49	6.05	L. inferior frontal gyrus, WM	
	-56	22	8	2,986	5.78	5.46	L. inferior frontal gyrus	
	-36	56	16	357	4.81	4.62	L. superior frontal gyrus, GM	10
	-24	56	4	357	4.39	4.24	L. superior frontal gyrus, WM	ROI9
	-28	54	24	357	4.29	4.15	L. superior frontal gyrus, WM	ROI10

R. right, L. left

Table 6 Summaries of the common and different regions from Tables 2 and 3 for the mean diffusivity (MD)

Region	
Common regions (AD > MCI)	
ROI1	R. superior temporal gyrus, WM R. temporal subgyrus, WM R. superior temporal gyrus, GM
ROI2	L. limbic parahippocampal gyrus, WM
Different regions (AD > MCI)	
gmMD	R. occipital subgyrus, WM L. superior frontal gyrus, GM L. medial frontal gyrus, WM
nMD	R. middle occipital gyrus, WM
pMD (ROI3)	R. middle temporal gyrus, WM R. and L. medial frontal gyrus, GM and WM
ROI4	R. occipital cuneus, WM L. parietal supramarginal gyrus, WM L. interior parietal lobule, WM L. limbic parahippocampal gyrus, GM
ROI5	L. limbic uncus, WM R. sublobar insula
Common regions (AD > CN)	
ROI2	L. limbic parahippocampal gyrus, WM
ROI3	R. middle temporal gyrus, WM
Different regions (AD > CN)	
gmMD	L. limbic uncus, GM, Amygdala R. and L. temporal subgyrus, WM
nMD	R. and L. temporal subgyrus, WM R. sublobar insula, GM
pMD	R. temporal subgyrus, WM
ROI4	R. occipital cuneus, WM R. occipital subgyrus, WM R. inferior occipital gyrus, WM

R. right, L. left

the diffusion-sensitizing gradients with different polarity, and the findings further support our hypothesis that intrinsic susceptibility variations of the brain contribute to the regional diffusion abnormalities in AD patients.

One of our findings was that the regional distribution of elevated gmMD values in the AD patients did not completely overlap with the corresponding pattern of nMD and pMD variations in the AD patients. The regional difference could reflect the heterogeneity of AD pathology or different stages of the disease, as well as the variations in the processes leading to local variations in magnetic susceptibility. For example, the regions where all three diffusion measurements (pMD, nMD, and gmMD) show significant alterations might be related to alterations primarily in the cell density that alter the MD, but they do not substantially alter the magnet susceptibility. On the

Table 7 Summaries of the common and different regions from Tables 2 and 3 for fractional anisotropy (FA)

Region	
Common regions (AD > MCI)	
No common region	
Different regions (AD > MCI)	
pFA (ROI 6,7,8)	R. and L. superior temporal gyrus, WM L. inferior frontal gyrus, GM R. sublobar extranuclear, WM R. sublobar insula, GM and WM R. limbic parahippocampal gyrus, WM R. temporal fusiform gyrus, GM L. occipital cuneus, GM L. limbic posterior cingulate L. middle temporal gyrus, WM
Common regions (AD > CN)	
No common region	
Different regions (AD > CN)	
pFA ROI 9, 10	L. inferior frontal gyrus, WM L. superior frontal gyrus, GM and WM

R. right, L. left

other hand, the regions without a significant change in the gmMD, but that are with significant changes in the nMD and pMD, could mainly reflect the characteristic local magnetic susceptibility variations related to the paramagnetic effects from iron-rich processes involving the oligodendrocytes and amyloid plaques. The sensitivity differences between in the various MD maps cannot explain the regional discordance between the changes in the pMD and nMD. We cannot directly compare the sensitivity difference between the gmMD maps and the pMD or nMD maps because the gmMD map is derived by averaging two DT-MRI signals and generally has a higher signal-to-noise ratio than the individual pMD and nMD, which are based on a single DT-MRI signal. Therefore, the geometrically calculated MD (gmMD) in the AD or MCI patients may be better to differentiate accurately between the groups as compared to that obtained with the single polarity.

We tested our concepts in water phantom before we applied in human brain. The mean ADC value or average tensor components or mean eigenvalue is different about 0.00004 mm²/s, and the FA value is different about 0.00188 between the positive and negative diffusion gradients. This means that our human results should be clearly shown reliable measurements of DTI data without absence of any

Table 8 The ROI data and results of the corresponding statistical test for the mean diffusivity (MD) values

ROI	Subjects			<i>p</i> value				
	AD	MCI	CN	AD–MCI	AD–CN	MCI–CN		
Superior temporal gyrus, ROI1, X ±58, Y –6, z –4	Rt	gm	1.045±0.156	0.875±0.072	0.908±0.084	0.00026	0.00490	0.22578
	Rt	neg	1.049±0.161	0.870±0.076	0.907±0.091	0.00022	0.00500	0.21123
	Rt	pos	1.042±0.153	0.879±0.069	0.909±0.079	0.00030	0.00450	0.24897
	Lt	gm	1.023±0.155	0.911±0.117	0.955±0.099	0.02489	0.15434	0.25234
	Lt	neg	1.027±0.163	0.917±0.127	0.960±0.108	0.03755	0.18508	0.30315
	Lt	pos	1.022±0.150	0.907±0.110	0.954±0.092	0.01635	0.13488	0.19277
Limbic parahippocampal gyrus, ROI 2, X ±32, y –24, z –22	Rt	gm	0.100±0.111	0.891±0.071	0.882±0.060	0.00187	0.00091	0.69383
	Rt	neg	0.933±0.111	0.877±0.074	0.875±0.061	0.00112	0.00088	0.93385
	Rt	pos	1.007±0.111	0.906±0.074	0.890±0.058	0.00395	0.00088	0.49030
	Lt	gm	1.036±0.116	0.879±0.060	0.882±0.075	0.00002	0.00012	0.92913
	Lt	neg	1.031±0.111	0.868±0.058	0.870±0.074	0.00001	0.00005	0.94042
	Lt	pos	1.036±0.118	0.890±0.062	0.893±0.078	0.00008	0.00039	0.90633
Middle temporal gyrus, ROI 3, X ±40, y –74, z 28	Rt	gm	0.963±0.099	0.837±0.062	0.832±0.058	0.00011	0.00009	0.78235
	Rt	neg	0.963±0.108	0.832±0.062	0.836±0.062	0.00013	0.00034	0.89277
	Rt	pos	0.966±0.105	0.843±0.064	0.829±0.054	0.00025	0.00008	0.49316
	Lt	gm	0.944±0.115	0.852±0.059	0.875±0.078	0.00590	0.05985	0.33837
	Lt	neg	0.944±0.118	0.846±0.065	0.871±0.077	0.00511	0.05068	0.30961
	Lt	pos	0.947±0.114	0.859±0.054	0.879±0.081	0.01048	0.14942	0.23174
Occipital cuneus, ROI 4, X ±26, y –84, z 16	Rt	gm	0.948±0.090	0.829±0.051	0.839±0.058	0.00004	0.00035	0.61712
	Rt	neg	0.934±0.082	0.828±0.059	0.839±0.060	0.00015	0.00085	0.59032
	Rt	pos	0.962±0.106	0.830±0.046	0.838±0.057	0.00004	0.00031	0.65473
	Lt	gm	0.924±0.103	0.853±0.080	0.879±0.063	0.03507	0.15081	0.31487
	Lt	neg	0.920±0.104	0.853±0.087	0.873±0.063	0.05182	0.13221	0.45565
	Lt	pos	0.927±0.107	0.853±0.075	0.884±0.064	0.02715	0.18312	0.21208
Limbic uncus, ROI 5, X ±24, y –4, z –32	Rt	gm	1.047±0.142	0.950±0.103	0.928±0.066	0.03111	0.00532	0.46841
	Rt	neg	1.040±0.165	0.933±0.111	0.918±0.081	0.03475	0.01353	0.65553
	Rt	pos	1.053±0.135	0.967±0.100	0.943±0.065	0.04522	0.00692	0.42162
	Lt	gm	1.055±0.118	0.962±0.071	0.912±0.097	0.00053	0.00090	0.61871
	Lt	neg	1.053±0.119	0.912±0.074	0.899±0.099	0.00023	0.00049	0.66891
	Lt	pos	1.062±0.124	0.939±0.069	0.923±0.098	0.00118	0.00166	0.57150

Rt right, Lt left, AD Alzheimer's disease, MCI mild cognitive impairment, CN cognitive normal, Gm geometric mean, neg negative, p positive
The ROIs are listed in the table above. The significant level was used with $p=0.016$ ($p=0.05/3$ times repeated) because we repeated the same tasks three times among the three groups

systematic bias due to the different gradient settings (positive vs negative).

In voxel-wise comparisons of human brain data, the results from geometric mean appear highly similar to those from negative gradients, while positive gradients show very different results. We may explain the reason as the following. The largest contribution of cross terms tends to be when the applied diffusion gradient and the intrinsic background magnetic field gradient are in the same direction and sign as the frequency-encoding direction. With the used TE value, this would mean that we would get more positive pixels for positive diffusion and read

gradients than for negative diffusion and positive read gradients. This is supported by getting comparable diffusion rates for all gradient directions on an isotropic phantom experiment with the same acquisition parameters.

Our DTI findings using diffusion-sensitizing gradients with the single positive polarity are largely consistent with the findings of the previous DT-MRI studies that used a single gradient polarity [1, 3–5, 27]. Specifically, our finding in AD patients of increased pMD values in the right middle temporal gyrus white matter and the left superior temporal gyrus white matter, as compared to that of the MCI patients, are consistent with a previous report

Table 9 The ROI data and results of the corresponding statistical test for the fractional anisotropy (FA) values

ROI	Subjects			<i>p</i> value				
	AD	MCI	CN	AD–MCI	AD–CN	MCI–CN		
Superior temporal gyrus, ROI 6, x ±58, y –32, z +14	Rt	gm	0.238±0.015	0.225±0.014	0.233±0.034	0.02207	0.65877	0.35914
	Rt	neg	0.293±0.022	0.269±0.014	0.280±0.036	0.00077	0.24791	0.23248
	Rt	pos	0.292±0.027	0.269±0.016	0.276±0.046	0.00467	0.25159	0.54348
	Lt	gm	0.227±0.016	0.204±0.014	0.213±0.016	0.00014	0.02329	0.10851
	Lt	neg	0.282±0.026	0.250±0.017	0.266±0.021	0.00024	0.07557	0.02310
	Lt	pos	0.296±0.027	0.255±0.020	0.267±0.023	0.00002	0.00341	0.12132
Superior temporal gyrus, ROI 7, x ±64, y –16, z –6	Rt	gm	0.212±0.023	0.190±0.013	0.194±0.012	0.00105	0.00807	0.32091
	Rt	neg	0.264±0.028	0.237±0.014	0.246±0.020	0.00137	0.04480	0.18303
	Rt	pos	0.271±0.036	0.236±0.015	0.244±0.018	0.00062	0.01191	0.14461
	Lt	gm	0.120±0.017	0.190±0.016	0.181±0.019	0.10116	0.00693	0.13342
	Lt	neg	0.251±0.015	0.240±0.021	0.233±0.029	0.12077	0.04121	0.40239
	Lt	pos	0.265±0.036	0.238±0.015	0.229±0.021	0.00667	0.00202	0.18436
Superior temporal gyrus, ROI 8, x ±58, y –26, z –4	Rt	gm	0.231±0.023	0.210±0.016	0.217±0.234	0.00477	0.11993	0.29256
	Rt	neg	0.276±0.026	0.254±0.021	0.265±0.030	0.01128	0.31982	0.19190
	Rt	pos	0.284±0.032	0.249±0.013	0.262±0.028	0.00018	0.05107	0.08649
	Lt	gm	0.223±0.026	0.218±0.020	0.220±0.020	0.55759	0.67971	0.85453
	Lt	neg	0.270±0.020	0.266±0.026	0.268±0.029	0.62074	0.84838	0.80622
	Lt	pos	0.281±0.030	0.263±0.018	0.269±0.026	0.03818	0.22205	0.44215
Superior frontal gyrus, ROI 9, x ±24, y +56, z +4	Rt	gm	0.253±0.027	0.255±0.026	0.254±0.033	0.87967	0.93917	0.95524
	Rt	neg	0.303±0.022	0.293±0.023	0.301±0.033	0.24157	0.90915	0.40468
	Rt	pos	0.311±0.030	0.302±0.036	0.295±0.030	0.47368	0.15143	0.51314
	Lt	gm	0.268±0.025	0.244±0.027	0.247±0.025	0.01453	0.02980	0.73554
	Lt	neg	0.311±0.026	0.289±0.034	0.302±0.030	0.05134	0.39898	0.24469
	Lt	pos	0.347±0.045	0.303±0.034	0.298±0.030	0.00298	0.00125	0.67386
Superior frontal gyrus, ROI 10, x ±28, y +58, z +24	Rt	gm	0.205±0.027	0.188±0.027	0.182±0.028	0.08842	0.03057	0.54784
	Rt	neg	0.249±0.042	0.235±0.032	0.235±0.033	0.28368	0.30211	0.98821
	Rt	pos	0.279±0.046	0.248±0.041	0.239±0.037	0.04714	0.01125	0.49593
	Lt	gm	0.203±0.027	0.178±0.027	0.168±0.042	0.00985	0.00989	0.44181
	Lt	neg	0.258±0.028	0.229±0.036	0.223±0.052	0.01580	0.02985	0.73585
	Lt	pos	0.272±0.039	0.241±0.045	0.221±0.057	0.05028	0.00800	0.26447

Rt right, *Lt* left, *AD* Alzheimer's disease, *MCI* mild cognitive impairment, *CN* cognitive normal, *Gm* geometric mean, *neg* negative, *p* positive
The ROIs are listed in the table above. The significant level was used with $p=0.016$ ($p=0.05/3$ times repeated) because we repeated the same tasks three times among the three groups

[5]. Similarly, our results in AD patients of increased pMD values in the limbic parahippocampal gyrus white matter, the right temporal gyrus white matter, and the right occipital white matter are consistent with the results of the previous studies [1, 3, 4, 27].

Previous studies have also demonstrated that the background gradient effects in DT-MRI can be amplified due to an interaction (also known as the “cross-term effect”) between the external and background gradients. Several diffusion studies have reported significant cross-term effects on the measurements of the apparent diffusion coefficients (ADC) in phantoms [28], rat brain [14], and pig

spinal cord [29]. Indeed, several studies have shown that cross-term effects can also depend, at least in part, on the types of sequence and the external gradient patterns [30, 31], and these effects can in principle be minimized by the combined use of a multispin-echo preparation and pulse gradients for diffusion encoding [32] or the combined use of asymmetric bipolar diffusion-encoding gradients and twice refocused spin-echo preparation [22]. A further class of experimental strategies that also accounts for the presence of field inhomogeneities is based on the use of bipolar gradient pluses [22, 33, 34]. However, some ADC studies have found no detectable cross-term effects [35],

including a DT-MRI study in normal young human brain [36]. Our results generalize the cross-term findings by demonstrating that the effect can substantially vary between different brain conditions. Our results in AD patients that not all the variations in the pMD or nMD maps were also present in the gmMD maps emphasize the importance of accounting for the background gradients when comparing the DT-MRI data between groups with different brain conditions. In particular, the findings indicate that a bias toward increased MD variability can be introduced if the background gradients are not considered. For the FA index, there were no differences between the positive and negative acquisitions. This is not surprising because FA is derived by taking the ratios of the eigenvalues. The sensitivity to detect an effect on FA is substantially diminished as compared to that of MD, which is simply the average of the eigenvalues.

Finally, although some previous investigators [2, 37, 38] have found significant differences of FA and MD between the MCI and CN patients, we did not find any significant differences for either FA or MD between these two groups. One explanation is that the MCI subjects in this study were only mildly impaired, as was reflected by their average MMSE score, which did not significantly differ from the score of the normal subjects. Another possibility is that our MCI group included only a few subjects with preclinical AD pathology as compared to that of the MCI groups in the other previous studies.

In general, the FA values in the white matter can be contaminated by signal from CSF spaces, which are more pronounced in AD than in CN subject. This will support increased MD and decreased FA values which showed several previous papers. However, in our study, we use the CSF-suppressed DTI method to minimize partial volume effect. Increased MD values in a voxel may be not directly related to CSF contamination. We think that this may be related to loss of integrity of neuronal structure. In this case, FA value can also decrease or increase dependent on the types of neuronal loss in the voxel. Previous findings of decreased FA in AD may be due to (1) neuronal loss in the voxel (microstructural changes) or (2) increased contributions of CSF signals caused by loss of cortical GM (atrophy; macroscopic changes) because many of previous studies did not use an inversion-recovery DTI sequence. A lot of CSF signals may be contributed to decreased FA values in AD in the previous findings. However, previous and our findings of increased FA in AD may be due to loss selectively in a certain direction rather than every neuron in the voxel (selective neuronal loss and microstructural changes). In addition, our finding of increased FA in AD may be additionally due to less contribution of CSF signals. If brain atrophy is contributed to FA changes, then our finding may be unrelated to microstructural alternation. The recent paper has shown increased FA values in those

patients, although they did not use any kinds of CSF suppression techniques. Teipel et al. found increased FA values in AD patients compared with elderly controls [39]. This increased FA values in AD may be associated with a decrease in crossing fibers or other nonparallel organization [40]. Teipel et al. [39] also found decreased FA values in AD patients compared with elderly control, but not in the present study. The largest difference between two studies is the selection of a statistical threshold. Teipel et al. [39] used uncorrected p value=0.01, but we used FDR-corrected p value=0.01 to consider multiple comparisons to reduce the false-positive findings. When we reinvestigated the results with the uncorrected p value=0.01, then we also found decreased FA values in AD patients compared with elderly control in the temporal and frontal lobes which were similar findings from Teipel et al. [39]. In addition, there is usually more gray matter loss in AD than in elderly normal subjects. Within a voxel which composes both gray matter and white matter, FA in our study can also be increased when there is gray matter loss without changing white matter volume because we acquired DTI data with suppressing signals from the brain atrophy. In this case, the relative contribution of white matter in the voxel can be increased. In general, people have been found increased MD and decreased FA in AD compared with normal. This decreased FA may only represent increased atrophy in a certain voxel because people have analyzed their FA data without correcting the atrophy contribution. In this study, we used an inversion-recovery DT-MRI sequence, which minimize the CSF contamination in a voxel. During FA analysis, we may find tissue alternations in the voxel, independent on the contributions of brain atrophy, which usually happens in gray matter. Therefore, it may be very important to correct the brain atrophy before analyzing FA maps, especially obtained FA maps in patients with AD.

In this study, MD values in some ROIs are higher in CN than in MCI. FA values in some ROIs are higher in MCI than in CN. We cannot clearly explain why this happens. However, we may think as the following: Although we divided the subject groups as MCI and CN based on the full neuropsychologic tests, the MMSE score does not significantly differ between two groups. In addition, although there is no significant difference of age between two groups, the MCI group is relatively younger than the CN group. As we found the results based on both the voxel-wise and the ROI-based comparisons, there were no significant differences any indices between two groups. Although several previous studies found increased MD values and decreased FA values in AD compared with CN, some studies also did not found any differences between MCI and CN groups for both indices [40]. In this case, the pathological changes in some areas in AD may not yet

affect individuals with MCI. Furthermore, as we can see in Table 8, MD values in MCI are higher than those in CN in the right limbic parahippocampal gyrus, in the left middle temporal gyrus, and in the right and left limbic uncus, as expected. In addition, as we can see in Table 9, FA values in most ROIs are higher in CN than those in MCI, especially in the right and left superior temporal gyrus, as expected. The pathological changes in those areas may start to affect individuals with MCI. This may indicate regional variations of MD and FA values in patients with MCI compared with CN subjects.

Several limitations of our study ought to be mentioned. Firstly, none of the AD patient had a definite diagnosis confirmed by autopsy. Therefore, the DTI alterations in the AD patients might not be related to AD at all. Another limitation is that we did not investigate the spatially variant background gradients for the higher order diffusion effects, such as kurtosis. Therefore, the contributions from these other effects might have biased our results. Another technical limitation is that the geometrical average maps, which are derived by averaging two signals, have a higher SNR than do the individual maps of diffusivity without averaging, and this leads to differences in sensitivity. Therefore, the findings of regional discrepancies between these maps are difficult to interpret. Finally, in this study, we mainly used a voxel-based analysis of the DTI indices of both MD and FA maps. Currently, the voxel-based analysis is still under investigating in optimization processing of DT-MRI data. Although the voxel-based analysis can be used a whole brain investigation without having a specific hypothesis, the results may be altered by several factors, such as a spatial normalization of DT-MRI data acquired with an EPI sequence, a coregistration between anatomic magnetic resonance images and maps of DTI indices, a filter size of smoothing kernel, and/or registration of individual MD or FA maps onto a common space. Therefore, optimizations of the preprocessing and postprocessing steps are required to minimize any errors during processing [41, 42].

Conclusions

Accurate DT-MRI measurements require considering the effects from background gradients, and especially in patients with pathological brain conditions such as AD. Furthermore, geometric average diffusion measures (e.g., gmMD) can be useful to minimize the intrinsic local magnetic susceptibility variations in brain tissue. As we demonstrated for the case of AD, these maps may provide complementary information to the standard DTI maps.

Acknowledgments We thank Dr. Michal Neeman at Weizmann Institute in Rehovot, Israel, for his valuable comments. This research was supported by a grant of the Korean Health 21 R&D Project, Ministry of Health and Welfare, Republic of Korea (A062284).

Conflict of interest We declare that we have no conflict of interest.

Open Access This article is distributed under the terms of the Creative Commons Attribution Noncommercial License which permits any noncommercial use, distribution, and reproduction in any medium, provided the original author(s) and source are credited.

References

- Duan JH, Wang HQ, Xu J, Lin X, Chen SQ, Kang Z, Yao ZB (2006) White matter damage of patients with Alzheimer's disease correlated with the decreased cognitive function. *Surg Radiol Anat* 28:150–156
- Medina D, DeToledo-Morrell L, Urresta F, Gabrieli JD, Moseley M, Fleischman D, Bennett DA, Leurgans S, Turner DA, Stebbins GT (2006) White matter changes in mild cognitive impairment and AD: a diffusion tensor imaging study. *Neurobiol Aging* 27:663–672
- Naggara O, Oppenheim C, Rieu D, Raoux N, Rodrigo S, Dalla Barba G, Meder JF (2006) Diffusion tensor imaging in early Alzheimer's disease. *Psychiatry Res* 146:243–249
- Rose SE, Janke AL, Chalk JB (2008) Gray and white matter changes in Alzheimer's disease: a diffusion tensor imaging study. *J Magn Reson Imaging* 27:20–26
- Stahl R, Dietrich O, Teipel SJ, Hampel H, Reiser MF, Schoenberg SO (2007) White matter damage in Alzheimer disease and mild cognitive impairment: assessment with diffusion-tensor MR imaging and parallel imaging techniques. *Radiology* 243:483–492
- Zhang Y, Schuff N, Jahng GH, Bayne W, Mori S, Schad L, Mueller S, Du AT, Kramer JH, Yaffe K, Chui H, Jagust WJ, Miller BL, Weiner MW (2007) Diffusion tensor imaging of cingulum fibers in mild cognitive impairment and Alzheimer disease. *Neurology* 68:13–19
- Chua TC, Wen W, Slavin MJ, Sachdev PS (2008) Diffusion tensor imaging in mild cognitive impairment and Alzheimer's disease: a review. *Curr Opin Neurol* 21:83–92
- Nakata Y, Sato N, Abe O, Shikakura S, Arima K, Furuta N, Uno M, Hirai S, Masutani Y, Ohtomo K, Aoki S (2008) Diffusion abnormality in posterior cingulate fiber tracts in Alzheimer's disease: tract-specific analysis. *Radiat Med* 26:466–473
- Mielke MM, Kozauer NA, Chan KC, George M, Toroney J, Zerrate M, Bandeen-Roche K, Wang MC, Vanzijl P, Pekar JJ, Mori S, Lyketsos CG, Albert M (2009) Regionally-specific diffusion tensor imaging in mild cognitive impairment and Alzheimer's disease. *Neuroimage* 46:47–55
- Huang J, Friedland RP, Auchus AP (2007) Diffusion tensor imaging of normal-appearing white matter in mild cognitive impairment and early Alzheimer disease: preliminary evidence of axonal degeneration in the temporal lobe. *AJNR Am J Neuroradiol* 28:1943–1948
- Roth AD, Ramirez G, Alarcon R, Von Bernhardi R (2005) Oligodendrocytes damage in Alzheimer's disease: beta amyloid toxicity and inflammation. *Biol Res* 38:381–387
- Schmitz T, Chew LJ (2008) Cytokines and myelination in the central nervous system. *Scientific World J* 8:1119–1147

13. Bartzokis G (2004) Age-related myelin breakdown: a developmental model of cognitive decline and Alzheimer's disease. *Neurobiol Aging* 25:5–18, Author reply 49–62
14. Does MD, Zhong J, Gore JC (1999) In vivo measurement of ADC change due to intravascular susceptibility variation. *Magn Reson Med* 41:236–240
15. Connor JR, Menzies SL, St Martin SM, Mufson EJ (1992) A histochemical study of iron, transferrin, and ferritin in Alzheimer's diseased brains. *J Neurosci Res* 31:75–83
16. Smith MA, Wehr K, Harris PL, Siedlak SL, Connor JR, Perry G (1998) Abnormal localization of iron regulatory protein in Alzheimer's disease. *Brain Res* 788:232–236
17. Smith MA, Harris PL, Sayre LM, Perry G (1997) Iron accumulation in Alzheimer disease is a source of redox-generated free radicals. *Proc Natl Acad Sci USA* 94:9866–9868
18. Neeman M, Freyer JP, Sillerud LO (1991) A simple method for obtaining cross-term-free images for diffusion anisotropy studies in NMR microimaging. *Magn Reson Med* 21:138–143
19. Jara H, Wehrli FW (1994) Determination of background gradients with diffusion MR imaging. *J Magn Reson Imaging* 4:787–797
20. Petersen RC, Smith GE, Waring SC, Ivnik RJ, Tangalos EG, Kokmen E (1999) Mild cognitive impairment: clinical characterization and outcome. *Arch Neurol* 56:303–308
21. Hirsch JG, Bock M, Essig M, Schad LR (1999) Comparison of diffusion anisotropy measurements in combination with the flair-technique. *Magn Reson Imaging* 17:705–716
22. Reese TG, Heid O, Weisskoff RM, Wedeen VJ (2003) Reduction of eddy-current-induced distortion in diffusion MRI using a twice-refocused spin echo. *Magn Reson Med* 49:177–182
23. Jones DK, Horsfield MA, Simmons A (1999) Optimal strategies for measuring diffusion in anisotropic systems by magnetic resonance imaging. *Magn Reson Med* 42:515–525
24. Ashburner J, Friston KJ (1999) Nonlinear spatial normalization using basis functions. *Hum Brain Mapp* 7:254–266
25. Ashburner J, Friston KJ (2000) Voxel-based morphometry—the methods. *Neuroimage* 11:805–821
26. Schwartzman A, Dougherty RF, Taylor JE (2008) False discovery rate analysis of brain diffusion direction maps. *Ann Appl Stat* 2:153–175
27. Fellgiebel A, Wille P, Muller MJ, Winterer G, Scheurich A, Vucurevic G, Schmidt LG, Stoeter P (2004) Ultrastructural hippocampal and white matter alterations in mild cognitive impairment: a diffusion tensor imaging study. *Dement Geriatr Cogn Disord* 18:101–108
28. Price WS, Stilbs P, Jonsson B, Soderman O (2001) Macroscopic background gradient and radiation damping effects on high-field PGSE NMR diffusion measurements. *J Magn Reson* 150:49–56
29. Trudeau JD, Dixon WT, Hawkins J (1995) The effect of inhomogeneous sample susceptibility on measured diffusion anisotropy using NMR imaging. *J Magn Reson B* 108:22–30
30. Duh A, Mohoric A, Stepisnik J, Sersa I (2003) The elimination of magnetic susceptibility artifacts in the micro-image of liquid-solid interfaces: internal gradient modulation by the CPMG RF train. *J Magn Reson* 160:47–51
31. Sorland GH, Aksnes D, Gjerdaker L (1999) A pulsed field gradient spin-echo method for diffusion measurements in the presence of internal gradients. *J Magn Reson* 137:397–401
32. van Dusschoten D, Moonen CT, de Jager PA, Van As H (1996) Unraveling diffusion constants in biological tissue by combining Carr-Purcell-Meiboom-Gill imaging and pulsed field gradient NMR. *Magn Reson Med* 36:907–913
33. Hong DTX (1992) Measuring diffusion in inhomogeneous systems in imaging mode using antisymmetric sensitizing gradients. *J Magn Reson* 99:561–570
34. Sun PZ, Seland JG, Cory D (2003) Background gradient suppression in pulsed gradient stimulated echo measurements. *J Magn Reson* 161:168–173
35. Beaulieu C, Allen PS (1996) An in vitro evaluation of the effects of local magnetic-susceptibility-induced gradients on anisotropic water diffusion in nerve. *Magn Reson Med* 36:39–44
36. Clark CA, Barker GJ, Tofts PS (1999) An in vivo evaluation of the effects of local magnetic susceptibility-induced gradients on water diffusion measurements in human brain. *J Magn Reson* 141:52–61
37. Rose SE, McMahon KL, Janke AL, O'Dowd B, de Zubicaray G, Strudwick MW, Chalk JB (2006) Diffusion indices on magnetic resonance imaging and neuropsychological performance in amnesic mild cognitive impairment. *J Neurol Neurosurg Psychiatry* 77:1122–1128
38. Cho H, Yang DW, Shon YM, Kim BS, Kim YI, Choi YB, Lee KS, Shim YS, Yoon B, Kim W, Ahn KJ (2008) Abnormal integrity of corticocortical tracts in mild cognitive impairment: a diffusion tensor imaging study. *J Korean Med Sci* 23:477–483
39. Teipel SJ, Stahl R, Dietrich O, Schoenberg SO, Pernecky R, Bokde AL, Reiser MF, Moller HJ, Hampel H (2007) Multivariate network analysis of fiber tract integrity in Alzheimer's disease. *Neuroimage* 34:985–995
40. Stebbins GT, Murphy CM (2009) Diffusion tensor imaging in Alzheimer's disease and mild cognitive impairment. *Behav Neurol* 21:39–49
41. Abe O, Takao H, Gono W, Sasaki H, Murakami M, Kabasawa H, Kawaguchi H, Goto M, Yamada H, Yamasue H, Kasai K, Aoki S, Ohtomo K (2010) Voxel-based analysis of the diffusion tensor. *Neuroradiology* 52:699–710
42. Kakeda S, Korogi Y (2010) The efficacy of a voxel-based morphometry on the analysis of imaging in schizophrenia, temporal lobe epilepsy, and Alzheimer's disease/mild cognitive impairment: a review. *Neuroradiology* 52:711–721